Regulation of 2D Arm Stability Against Unstable, Damping-Defined Environments in Physical Human-Robot Interaction

Fatemeh Zahedi, Tanner Bitz, Connor Phillips, and Hyunglae Lee*, *Member, IEEE*

***Abstract*— This paper presents an experimental study to investigate how humans interact with a robotic arm simulating primarily unstable, damping-defined, mechanical environments, and to quantify lower bounds of robotic damping that humans can stably interact with. Human subjects performed posture maintenance tasks while a robotic arm simulated a range of negative damping-defined environments and transiently perturbed the human arm to challenge postural stability. Analysis of 2-dimensional kinematic responses in both the time domain and phase space allowed us to evaluate stability of the coupled human-robot system in both anterior-posterior (AP) and medial-lateral (ML) directions, and to determine the lower bounds of robotic damping for stable physical human-robot interaction (pHRI). All subjects demonstrated higher capacity to stabilize their arm against negative damping-defined environments in the AP direction than the ML direction, evidenced by all 3 stability measures used in this study. Further, the lower bound of robotic damping for stable pHRI was more than 3.5 times lower in the AP direction than the ML direction: -30.0 Ns/m and -8.2 Ns/m in the AP and ML directions, respectively. Sensitivity analysis confirmed that the results in this study were relatively insensitive to varying experimental conditions. Outcomes of this study would allow us to design a less conservative robotic impedance controller that utilizes a wide range of robotic damping, including negative damping, and achieves more transparent and agile operations without compromising coupled stability and safety of the human-robot system, and thus improves the overall performance of pHRI.**

I. Introduction

Robotic arms or manipulators that physically interact with humans have gained high popularity in recent years and have been widely utilized in medical and industrial settings [1, 2]. When controlling physically interactive robots, including robotic arms, it is critical to create a control system that guarantees stable and safe physical human-robot interaction (pHRI) without neglecting or sacrificing performance. Many controllers have been introduced to address stability and safety [3-5], and one of the most efficient and robust ways is to regulate dynamic behavior at the point of interaction, i.e., mechanical impedance [6, 7], which describes energy exchanges between the human and the robot.

While it is quite common to heuristically select and tune parameters of a robotic impedance (or admittance) controller, such as Cartesian impedance at the end-effector (i.e., endpoint impedance), there also have been some efforts to estimate or quantify impedance of the human arm and integrate this knowledge into robotic impedance controllers [8, 9]. Indeed, there have been many studies on how human arm impedance is modulated and controlled during static posture and dynamic movement tasks [10-12]. Most studies have focused on the estimation of endpoint arm stiffness, the static component of arm impedance, and have demonstrated that the human central nervous system is capable of controlling endpoint stiffness in both predictive and reactive manners depending on the type of motor tasks and environmental conditions [13-16].

Compared to arm stiffness, arm viscosity or damping, another important component of the arm impedance, has been relatively understudied. This is due in part to technical challenges in estimating the intrinsic damping of the human arm[10]. The limited knowledge on how human arm damping is modulated and controlled during physical interaction limits its application to robotic impedance controllers. Thus, robotic damping of an impedance controller is primarily determined such that it exhibits highly dissipative behaviors to the human user. While this approach guarantees coupled stability and safety of the human-robot system, it is often excessively conservative, resulting in reduced transparency, agility, and decreased overall performance.

If human arm damping can be quantified, or if the lower bounds of robotic damping that humans can stably interact with are known, the impedance controller could utilize a wide range of robotic damping and achieve more transparent and agile operations without compromising coupled stability and safety of the human-robot system. For example, if human arm damping is known to be dissipative (i.e., positive damping), the robotic impedance controller could impose active damping (i.e., negative damping) over the period where robotic assistance is beneficial to the human user. As long as the magnitude of negative damping of the impedance controller is lower than that of human arm damping, this less conservative controller could preserve the coupled stability while improving overall performance, in particular, the transparency and agility, of pHRI.

With this goal in mind, this paper presents our recent efforts to investigate how stably humans can interact with a robotic arm simulating primarily unstable, damping-defined, mechanical environments, and to quantify lower bounds of robotic damping for stable pHRI. Rather than indirectly estimating the lower bounds based on system identification of human arm damping, we determined them directly by analyzing the kinematic responses of the arm during

Research supported by National Science Foundation Awards #1846885 and #1925110. Hyunglae Lee is with the School for Engineering of Matter, Transport, and Energy, Arizona State University, Tempe, AZ 85287, USA (e-mail: hyunglae.lee@asu.edu; *corresponding author: 480-727-7463; fax: 480-727-9321). Fatemeh Zahedi, Tanner Bitz, and Connor Phillips are with the School for Engineering of Matter, Transport, and Energy, Arizona State University, Tempe, AZ 85287, USA (e-mail: {fzahedi1, tbitz, cmphil13}@asu.edu).

interaction with a robotic arm that simulated damping-defined environments with different levels of stability.

We hypothesized that humans could stably interact with a robotic arm simulating negative damping to a certain lower limit. In addition, previous findings showing higher arm impedance in the anterior-posterior (AP) direction compared to the medial-lateral (ML) direction [11, 17] led us to hypothesize that the humans are more capable of stabilizing their arm in the AP direction than the ML direction. Thus, the lower bound of robotic damping for stable pHRI is lower in the AP direction than the ML direction. These hypotheses were tested through a set of human experiments. Subjects performed posture maintenance tasks while the robotic arm simulated a range of damping-defined mechanical environments each with different levels of stability. The robotic arm also transiently perturbed the human arm to challenge postural stability. Analysis of 2-dimensional (2D) kinematic responses allowed us to evaluate stability of the coupled human-robot system in both AP and ML directions, and to determine the lower bounds of robotic damping that humans can stably interact with.

II. Methods

A. Experimental Setup

A 7 degrees-of-freedom (DOF) robotic arm (LBR iiwa R820, KUKA, Germany) with a 6-axis load cell (Delta IP60, ATI Industrial Automation, NC) was used to evaluate 2D arm stability, i.e., AP and ML stability, during interaction with damping-defined mechanical environments with different levels of stability. Both kinematic and force data were recorded at 1 kHz.

Subjects were seated with their trunk securely strapped to a rigid chair, facing a feedback visual display at a distance of ~1 m (Fig. 1A). The feedback display, showing neutral and current hand positions, was provided to help subjects successfully complete visually-guided posture maintenance tasks (Fig. 1B). Subjects held the handle, which was connected to the robotic end-effector, with the shoulder in ~70° of abduction, ~45° of horizontal flexion, and the elbow in ~90° of flexion. This starting posture was considered the "neutral position" for all trials.

The robot was capable of simulating a range of mechanical environments as well as providing rapid position perturbations in both AP and ML directions. Two distinct controllers were implemented for this purpose. A position controller provided ramp position perturbations to disturb the arm posture either in the AP or ML direction. An admittance controller simulated a range of mechanical impedances (stiffness, damping and inertia) at the robotic end-effector [7]. Zero stiffness and constant mass were simulated in the horizontal plane, and only damping was varied to manipulate the level of damping-defined environmental stability. High stiffness of 10^6 N/m was simulated in the vertical plane to constrain vertical movement and maintain the subject's focus on 2D planar tasks.

During trials in the AP direction, variable damping values were simulated only in the AP direction, while damping in the ML direction was held constant at 30 Ns/m. The bounds of the variable damping changed between trials randomly and were selected in the range of [-50, 0] Ns/m with intervals of 10 Ns/m, except the last interval which was 20 Ns/m. Similarly, during trials in the ML direction, variable damping values were simulated only in the ML direction, while damping in the AP direction was held constant at 30 Ns/m. Again, the variable damping bounds changed randomly between trials, and were selected in the range of [-25, 0] Ns/m with intervals of 5 Ns/m, except the last interval which was 10 Ns/m. The range of simulated damping was determined based on preliminary experiments confirming that healthy subjects were unable to stabilize their arm in mechanical environment with damping less than -80 Ns/m and -40 Ns/m in the AP and ML directions, respectively.

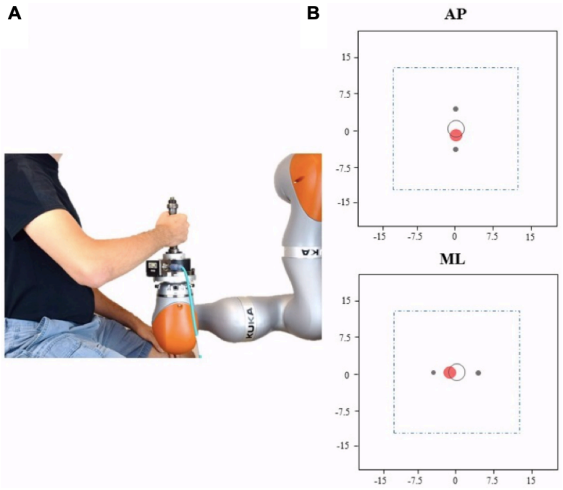

Fig. 1. Experimental setup. **A:** Side view of the robot coupled to a human subject. **B:** Visual feedback display. Black hollow and red solid circles were the neutral (±5 mm) and the current hand positions, respectively. Small gray circles were at ±5 cm from the neutral position and appeared at the beginning of each trial to help subjects explore the simulated mechanical environment. Dotted lines denote the boundaries of the virtual walls. (Top): Visual feedback for the AP direction trials. (Bottom): Visual feedback for the ML direction trials.

As a safety feature, a virtual wall of 26 x 26 cm^2 was implemented around the neutral position (Fig. 1B). When displacements reached the virtual wall, the simulated damping switched to 30 Ns/m to stabilize the arm and prevent any potential injuries.

For each trial, the robot alternated between the admittance controller and the position controller. The transition between controllers was completed in one sample time (1 ms). This small delay provided an almost instantaneous switch between controllers, allowing for transient perturbation of the arm while subjects interacted with the simulated mechanical environment.

B. Experimental Protocol

Fifteen young, healthy subjects (age: 19-27, height: 162-190 cm, weight: 47-90 kg, 11 males and 4 females) participated in this study, which was approved by the Institutional Review Board of Arizona State University (STUDY 00010123). Subjects provided informed, written consent prior to participation. All experimental procedures were performed in accordance with the relevant guidelines and regulations. No subject was informed regarding the hypotheses.

Two sets of experiments were performed on two separate days. All 15 subjects participated in the first experiment, where we determined lower bounds of robotic damping that humans can stably interact with. Twelve subjects, a subset of those in the first experiment, also participated in the second experiment, where we performed a sensitivity analysis to evaluate any confounding effects of the inertia simulated by the admittance controller and the perturbation profiles of the position controller on the lower bounds of robotic damping that were identified in the first experiment.

In the first experiment, subjects were instructed first to explore a randomly selected mechanical environment by reaching the small gray circles on the visual feedback display (Fig. 1B) that were 5 cm apart from the neutral position, and then to return to the neutral position (±5 mm). After the neutral position was maintained for a randomized time interval of 0.5-1.5 s, the position perturbation displaced the arm to challenge arm stability. Subjects were asked to move their arm back to the neutral position as efficiently as possible following the perturbation. There was a 3 s stabilizing period right after the perturbation, where subjects interacted with the original mechanical environment prior to the perturbation.

Zero stiffness and 10 kg mass were simulated in the horizontal plane for all experiments, and only damping was varied to manipulate the level of environmental stability. The position perturbation had an amplitude of 5 cm with an average speed and ending speed of 20 cm/s.

A total of 20 experimental conditions (5 damping × 4 perturbation) were tested. For trials in the AP direction (or ML direction), subjects were exposed to 5 distinct, damping-defined environments in the range of [-50, 0] Ns/m (or [-25, 0] Ns/m) and AP (or ML) position perturbations. Each experimental condition was repeated 12 times, resulting in a total of 240 trials. In order to avoid fatigue, the experiment was split into 12 blocks with at least a minute of rest between blocks. Two additional training blocks were included before the main experiment, which allowed subjects to familiarize themselves with the experimental setup and protocol, and to practice reaching the target under different mechanical environments. The entire experiment including these two training blocks took under 1 hour.

In the second experiment, 12 subjects were split into two groups to investigate if there exist any significant effects of simulated inertia (Group 1) and perturbation profile (Group 2) on the results of the first experiment. Six subjects in Group 1 performed the same posture maintenance tasks as in the first experiment, but under varying inertia conditions. Four different inertias (8, 10, 12, and 14 kg) of the admittance controller were tested for each of 5 different damping conditions. The same perturbation profile as in the first experiment was used.

The other six subjects in Group 2 performed the same stabilization task, but under different perturbation profile conditions. Four different ending perturbation velocities (10, 15, 20, and 25 cm/s) were tested for each of 5 different damping conditions. The simulated inertia was fixed to 10 kg.

For each group, each experimental condition was repeated 10 times in each of AP and ML directions, resulting in a total of 400 trials.

C. Data Analysis

Stability of the endpoint, i.e., stability at the contact point between the human arm and the robot, was quantified in both the time domain and phase space. In the time domain, the success rate of achieving stability and the time to regain stability were calculated for each experimental condition [18]. In the phase space, the rate of reducing the kinematic error after perturbation was calculated using the phase-space contraction method [19, 20].

If subjects had failed to stabilize the arm prior to the perturbation, meaning the hand position (endpoint) passed the boundaries of the virtual wall (±13 cm from the neutral position) during exploration of the simulated environment, the trial was considered a failed trial.

For successful trials in the exploration phase, the time to regain stability was calculated from the first moment that subjects maintained the hand position around the neutral position (±5 mm) for 500 ms continuously after the perturbation. If subjects had failed to meet this criterion within 3 s after the perturbation or if the hand position had passed the boundaries of the virtual walls, the trial was considered a failed trial and 3 s was assigned to the time to regain stability for further data analysis.

At the completion of the experiment, the rate of successful trials was calculated for each experimental condition. Further, the lowest bound of robotic damping in which the subjects could maintain stability (i.e., 100% success rate) was calculated for each perturbation direction.

For the phase-space contraction analysis, a 2D state vector $\vec{X} = [x \quad \dot{x}]$ was defined where x and $\dot{x}$ were position and velocity, respectively. Two state arrays, $\vec{X}(t)$ and $\vec{X}(t+1)$, were then defined as follows:

$$\vec{X}(t) = \begin{bmatrix} x(t_1) & \dot{x}(t_1) \\ x(t_2) & \dot{x}(t_2) \\ \vdots & \vdots \\ x(t_{n-1}) & \dot{x}(t_{n-1}) \end{bmatrix}, \vec{X}(t+1) = \begin{bmatrix} x(t_2) & \dot{x}(t_2) \\ x(t_3) & \dot{x}(t_3) \\ \vdots & \vdots \\ x(t_n) & \dot{x}(t_n) \end{bmatrix} \quad (1)$$

where t_1 was the moment when the perturbation was completed, and t_n was the first moment that subjects maintained the hand position around the neutral position (±5 mm) for 500 ms continuously after the perturbation, or 3 s if the trial had failed to achieve stability. In order to lessen the computational burden without losing details of the state trajectory in the phase plane, raw data of position and velocity (recorded at 1 kHz) were down sampled by averaging consecutive data points within a 50 ms window. Two state arrays with down-sampled data were denoted as $\vec{X}(k)$ and $\vec{X}(k+1)$, and their causal relationship can be described by a function f:

$$\vec{X}(k+1) = f(\vec{X}(k)) \quad (2)$$

Then, this potentially nonlinear relationship was linearized with respect to the origin (i.e., neutral position) and represented by a 2×2 Jacobian matrix J_f:

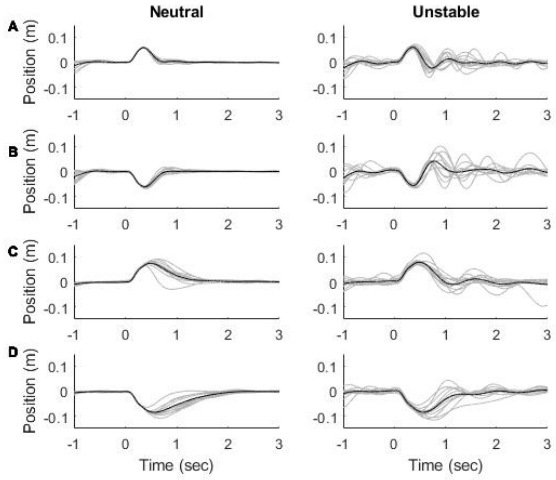

Fig. 2. Kinematic responses of the endpoint of a representative subject. Endpoint positions on the time interval of [-1, 3] s, where 0 s is the onset of the perturbation. **A:** anterior, **B:** posterior, **C:** medial, and **D:** lateral direction. (Left): robotic damping for the neutral environment is 0 Ns/m. (Right): robotic damping for the unstable environment is -50 and -25 Ns/m for the AP and ML directions, respectively. Gray traces represent individual trials, and bold trace is the average of all individual trials.

$$\vec{X}(k+1) = J_f \vec{X}(k) \quad (3)$$

The maximum eigenvalue of J_f was calculated to quantify the rate of contraction of the state trajectory in the phase space. The lower the maximum eigenvalue, the more stable the kinematic response.

The group results were averaged after evaluating the 3 stability measures (i.e., the success rate, time to regain stability, and maximum eigenvalue from the phase-space contraction analysis) for each individual subject. Statistical analyses were performed in order to test how these group results changed with the level of environmental stability. A one-way repeated measures ANOVA was performed separately for each of the 3 stability measures (dependent variables) followed by pairwise comparisons with Bonferroni correction. The level of environmental stability (or robotic damping value) was used as the within-subject factor. Separate analyses were performed for AP and ML directions.

Movement direction was used as the within-subject factor for the one-way repeated measures ANOVA analysis of the lower bound of robotic damping for stable interaction. All statistical tests were made using the SPSS statistical package.

For the sensitivity analysis, 3 stability measures were quantified in both varying inertia conditions (8, 10, 12, and 14 kg) and varying perturbation conditions (ending velocity of 10, 15, 20, and 25 cm/s). Specifically, the percentage difference between each condition and the average of 4 conditions was calculated:

$$\%Diff_i = \frac{|\text{condition}_i - (\sum_{i=1}^{4} \text{condition}_i)/4|}{(\sum_{i=1}^{4} \text{condition}_i)/4} \times 100 \quad (4)$$

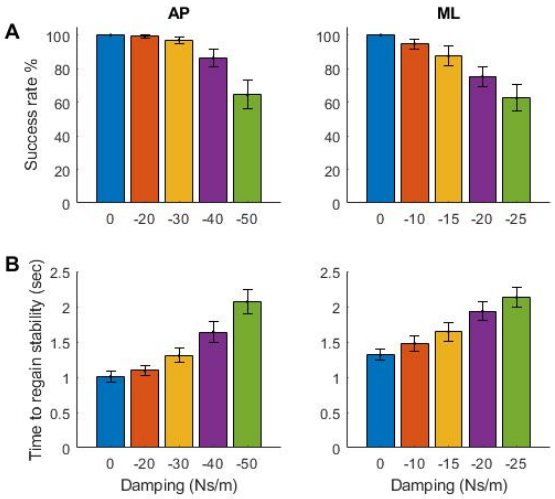

Fig. 3. Group results of the success rate and time to regain stability. (Left): AP direction, (Right): ML direction. **A:** Average success rate of achieving stability across all subjects. **B:** Average time to regain stability in AP (left column) and ML (right column) for 5 different robotic damping values in [-50, 0] Ns/m and [-25, 0] Ns/m for the AP and ML directions, respectively. Bars and error bars denote the mean and 95% confidence interval.

III. Results

All subjects in this study stably interacted with a robotic arm simulating negative damping to a certain degree of stability, but they used more time and effort to stabilize their arm as the level of environmental stability decreased (Fig. 2).

In both directions of movement, the success rate of achieving stability significantly decreased alongside the decrease of environmental stability ($p << 0.001$) (Fig. 3). When averaged across subjects, the success rate of achieving stability in the AP direction was higher than 96% in the robotic damping range of [-30 0] Ns/m. Pairwise comparison showed that results in -20 and -30 Ns/m were not statistically different ($p = 0.18$). At -50 Ns/m the success rate significantly decreased reaching 64%. Results in -40 Ns/m and -50 Ns/m were significantly different from those in any other four damping conditions ($p << 0.001$).

The success rate in the ML direction showed a similar trend. It was higher than 94% in the robotic damping range of [-10 0] Ns/m, but significantly decreased with the decrease of environmental stability. The success rates were 75% and 62% in -20 and -25 Ns/m, respectively. These values were significantly different from results in any other four damping conditions ($p << 0.001$).

While the time to regain stability significantly increased with the decrease of environmental stability in both movement directions ($p << 0.001$), it required substantially more time to stabilize the arm in the ML direction than the AP direction. At a damping value of -20 Ns/m, the times to regain stability were 1.10 s and 1.94 s for the AP and ML directions, respectively.

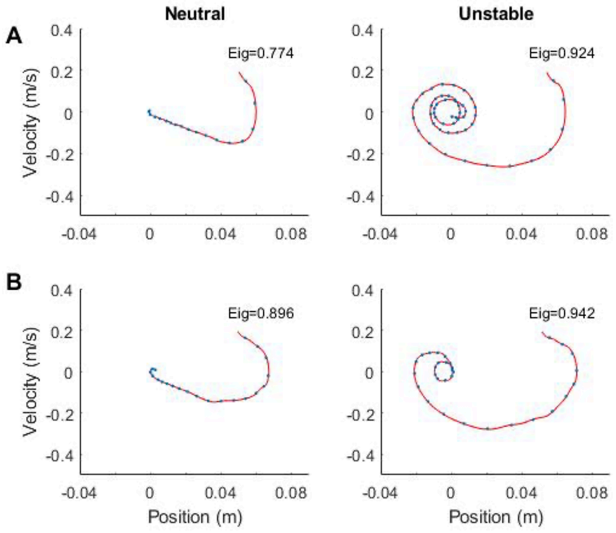

Fig. 4. Representative results of state trajectories (endpoint velocity vs. position) in the phase plane. **A**: AP direction, **B**: ML direction. (Left): robotic damping for the neutral environment is 0 Ns/m. (Right): robotic damping for the unstable environment is -50 Ns/m and -25 Ns/m for the AP and ML directions, respectively. Red traces represent raw data sampled at 1 kHz, and blue dot points represent down-sampled data points. The corresponding maximum eigenvalue was included in each plot.

TABLE I. LOWER BOUND OF THE ROBOTIC DAMPING THAT HUMANS CAN ALWAYS STABLY INTERACT WITH

Movement direction	Perturbation direction	Lower bound of robotic damping for stable pHRI (Ns/m)
AP	Anterior	-31.33 ± 9.15
	Posterior	-28.67 ± 12.46
ML	Medial	-7.67 ± 7.99
	Lateral	-8.67 ± 6.94

According to the phase-space contraction analysis, subjects had more difficulty in reducing the kinematic error induced by the position perturbation during interaction with a more unstable environment. Sample results of a representative subject showed higher overshoots, oscillations, and slower convergence to the neutral point with the decrease of environmental stability (Fig. 4). The maximum eigenvalue of the Jacobian matrix (J_f) clearly reflected this trend (Fig. 5); the maximum eigenvalue significantly increased with the decrease of environmental stability ($p << 0.001$). In addition, consistent with other stability measures in the time domain, the rate of reducing the kinematic error was faster (lower maximum eigenvalue) in the AP direction than the ML direction. Further, in the AP direction, there were clear changes in the maximum eigenvalue in the robotic damping range of [-30 0] Ns/m, but the rate of change was low in the range of [-50 -30] Ns/m. In the ML direction, while there was a clear change in the range of [-10 0] Ns/m, the rate of change was low in the range of [-25 -10] Ns/m.

There was a significant difference in the lower bound of robotic damping for stable pHRI between the AP and ML directions. While there was no statistical difference between

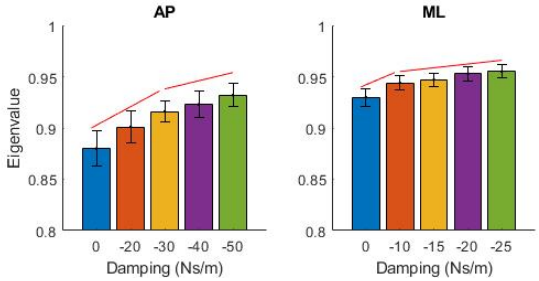

Fig. 5. Group results of the maximum eigenvalue from the phase-space contraction analysis. (Left): AP direction, (Right): ML direction. Bars and error bars denote the mean and 95% confidence interval. The red lines show the trend of changes across different robotic damping values.

TABLE II. SENSITIVITY ANALYSIS FOR VARYING INERTIA CONDITIONS

Success Rate				
	8 kg	10 kg	12 kg	14 kg
AP	3.4 (4.8)	1.0 (0.9)	1.8 (2.5)	3.8 (5.1)
ML	2.5 (2.3)	0.9 (0.5)	1.2 (1.0)	2.0 (1.6)
Time to Regain Stability				
	8 kg	10 kg	12 kg	14 kg
AP	6.3 (5.7)	1.4 (0.9)	3.9 (2.9)	6.1 (5.6)
ML	6.3 (3.1)	2.2 (1.3)	1.5 (0.8)	7.3 (3.9)
Maximum Eigenvalue				
	8 kg	10 kg	12 kg	14 kg
AP	1.7 (1.1)	0.7 (0.4)	0.8 (0.4)	1.6 (1.1)
ML	1.1 (0.5)	0.4 (0.4)	0.4 (0.4)	1.0 (0.4)

The mean and standard deviation (in parentheses) of all 5 damping conditions are reported.

TABLE III. SENSITIVITY ANALYSIS FOR VARYING PERTURBATION CONDITIONS

Success Rate				
	10 cm/s	15 cm/s	20 cm/s	25 cm/s
AP	1.7 (2.5)	1.0 (1.5)	0.8 (1.0)	1.8 (3.1)
ML	1.0 (1.0)	0.9 (1.1)	1.2 (1.8)	2.4 (4.1)
Time to Regain Stability				
	10 cm/s	15 cm/s	20 cm/s	25 cm/s
AP	5.1 (3.6)	3.7 (1.8)	3.6 (1.5)	6.7 (3.5)
ML	3.2 (2.0)	5.8 (3.3)	2.5 (2.3)	5.4 (3.1)
Maximum Eigenvalue				
	10 cm/s	15 cm/s	20 cm/s	25 cm/s
AP	0.7 (0.3)	0.5 (0.3)	0.3 (0.3)	0.4 (0.4)
ML	0.3 (0.2)	0.6 (0.4)	0.4 (0.3)	0.4 (0.3)

anterior and posterior perturbation conditions or medial and lateral conditions, the lower bound of damping was significantly lower in the AP direction than the ML direction ($p << 0.001$) (Table I). On average, subjects could interact stably with unstable environments simulating robotic damping of -30.0 Ns/m and -8.2 Ns/m in the AP and ML directions, respectively.

The sensitivity analysis showed a small influence of simulated inertia on the stability measures (Table II). When averaged across all 5 damping conditions, the $\%Diff_i$ (Eq. 4) for the success rate was less than 3.8% and 2.5% for AP and ML directions, respectively. The differences in time to regain stability were 6.3% (AP) and 7.3% (ML). Further, the difference for the maximum eigenvalue from the phase-space contraction analysis was less than 1.7% in any directions.

The effect of perturbation profile, specifically ending perturbation velocity, on the stability measures was also small (Table III). The $\%Diff_i$ for the success rate was less than 1.8% and 2.4% for AP and ML directions, respectively. The difference for the time to regain stability measure was 6.7% (AP) and 5.4% (ML). The difference for the maximum eigenvalue from the phase-space contraction analysis was less than 0.7% in any directions.

IV. Discussion

Compared to well-studied human arm stiffness, human arm damping, another important component of the human arm impedance, has been relatively understudied. This lack of knowledge limits the performance of robotic impedance controllers in pHRI, sometimes making them excessively conservative and in turn compromises transparency, agility, and the overall performance of the human-robot system.

Characterization and better understanding of human arm damping would allow us to identify the lower bounds of robotic damping that humans can stably interact with, and thus extend the utilization of robotic damping even to negative damping values. Robotic impedance controllers incorporating this new data would overcome the limitations of conservative (highly dissipative) impedance controllers [21].

Two primary goals of this study were 1) to investigate how humans interact with a robotic arm simulating primarily unstable, damping-defined, mechanical environments in a 2D space (i.e., AP and ML directions), and 2) to quantify lower bounds of robotic damping that humans can stably interact with. Rather than quantifying human arm damping, which has been known to be challenging, and indirectly estimating the lower bounds of robotic damping for stable pHRI, we determined these bounds directly by analyzing kinematic stability of the human arm during interaction with a robotic arm that simulated damping-defined environments with different levels of stability. We also ran a sensitivity analysis to evaluate any confounding effects of experimental conditions on the lower bounds of robotic damping for stable pHRI.

As hypothesized, experimental results demonstrated that subjects could stably interact with a robotic arm simulating negative damping to a certain degree of stability. In addition, all subjects have higher capacity to stabilize their arm against negative damping-defined environments in the AP direction than in the ML direction. This was evidenced by all stability measures used in this study. First, the success rate of achieving stability in the AP direction was higher than 96% when interacting with the robotic damping of -30 Ns/m, while the rate in the ML direction was lower than 63% during interaction with the robotic damping of -25 Ns/m. Second, for the same level of environmental stability (-20 Ns/m), the time to regain stability was about 2 times shorter in the AP direction than the ML direction. Third, consistent with results in the time domain, the rate of reducing the kinematic error, quantified by the maximum eigenvalue from the phase-space contraction analysis, was significantly faster (lower eigenvalue) in the AP direction than the ML direction. An additional paired t-test showed that the eigenvalue for the robotic damping of -50 Ns/m in the AP direction was even significantly lower than that for the robotic damping of -10 Ns/m in the ML direction (p = 0.013). Finally, the lower bound of robotic damping for stable pHRI was more than 3.5 times lower in the AP direction than the ML direction.

It is worth noting that higher capacity of arm stabilization in the AP direction than the ML direction is consistent with previous findings of significantly higher arm stiffness in the AP direction than the ML direction [11, 17]. Although not directly quantified in this study, previous studies demonstrating a strong correlation between joint stiffness and damping would suggest that arm damping was also significantly higher in the AP direction during the arm stabilization motor tasks [22, 23].

The sensitivity analysis with varying simulated inertias and perturbation profiles demonstrated that the results in this study were relatively insensitive to varying experimental conditions. It is also important to note that the experimental paradigm utilizing rapid position perturbations while subjects interacting with unstable mechanical environments is a very challenging situation for arm posture maintenance [15, 24]. Thus, one of the main conclusions in this study, in particular, the lower bound of robotic damping for stable pHRI was -30.0 Ns/m and -8.2 Ns/m in the AP and ML directions, would be used as conservative references in determining the lower bound of variable robotic impedance controllers.

Outcomes of this study, i.e., lower bounds of robotic damping that humans can stably interact in both the AP and ML directions, may be utilized to design a variable robotic impedance controller aimed at addressing the trade-off between agility/performance and stability in pHRI. In fact, our recent study to design a variable impedance controller for the human arm as well as for the human ankle have demonstrated that utilizing a wide range of robotic damping from negative to positive values could benefit both agility/performance and stability of the human-robot system [25, 26]. By further integrating the outcomes in this study, we can utilize a wider range of negative robotic damping in the AP direction than the ML direction to maximize the overall performance of the human-robot system without compromising its coupled stability.

Future research will include the quantification of the lower bounds of robotic damping for pHRI at various arm postures in a 3D space beyond the horizontal plane integration of this information into the design of variable robotic impedance controllers for robots interacting with the human arm in various applications, and evaluation of the effectiveness of the variable impedance controller in comparison with state-of-the-art passive/dissipative robotic controllers.

REFERENCES

[1] S. Haddadin, M. Suppa, S. Fuchs, T. Bodenmuller, A. Albu-Schaffer, and G. Hirzinger, *Towards the robotic co-worker* (Robotics Research). Springer, 2011, pp. 261-282.

[2] P. Tsarouchi, S. Makris, and G. Chryssolouris, "Human–robot interaction review and challenges on task planning and programming," *International Journal of Computer Integrated Manufacturing,* vol. 29, no. 8, pp. 916-931, 2016.

[3] A. Albu-Schaffer, S. Haddadin, C. Ott, A. Stemmer, T. Wimbock, and G. Hirzinger, "The DLR lightweight robot: design and control concepts for robots in human environments," *Industrial Robot-an International Journal,* vol. 34, no. 5, pp. 376-385, 2007.

[4] T. Yoshikawa, "Force control of robot manipulators," *In Proc. 2000 IEEE International Conference on Robotics and Automation,* pp. 220-226, 2000.

[5] S. Chiaverini, B. Siciliano, and L. Villani, "A survey of robot interaction control schemes with experimental comparison," *IEEE/ASME Trans on Mechatronics,* vol. 4, no. 3, pp. 273-285, 1999.

[6] N. Hogan, "Impedance Control - an Approach to Manipulation .1. Theory," *Journal of Dynamic Systems Measurement and Control-Transactions of the Asme,* vol. 107, no. 1, pp. 1-7, 1985.

[7] N. Hogan and S. P. Buerger, "Impedance and interaction control," *Robotics and Automation Handbook, New York, CRC Press,* 2005.

[8] S. P. Buerger and N. Hogan, "Complementary stability and loop shaping for improved human-robot interaction," *IEEE Transactions on Robotics,* vol. 23, no. 2, pp. 232-244, Apr 2007.

[9] T. Tsumugiwa, R. Yokogawa, and K. Hara, "Variable impedance control based on estimation of human arm stiffness for human-robot cooperative calligraphic task," in *IEEE International Conference on Robotics and Automation (ICRA)*, Washington D.C., USA, 2002, pp. 644-650.

[10] E. Burdet, R. Osu, D. W. Franklin, T. Yoshioka, T. E. Milner, and M. Kawato, "A method for measuring endpoint stiffness during multi-joint arm movements," *J Biomech,* vol. 33, no. 12, pp. 1705-9, Dec 2000.

[11] H. Gomi and R. Osu, "Task-dependent viscoelasticity of human multijoint arm and its spatial characteristics for interaction with environments," *J Neurosci,* vol. 18, no. 21, pp. 8965-78, Nov 1 1998.

[12] E. de Vlugt, A. C. Schouten, and F. C. T. van der Helm, "Closed-loop multivariable system identification for the characterization of the dynamic arm compliance using continuous force disturbances: a model study," *Journal of Neuroscience Methods,* vol. 122, no. 2, pp. 123-140, Jan 30 2003.

[13] E. J. Perreault, R. F. Kirsch, and A. M. Acosta, "Multiple-input, multiple-output system identification for characterization of limb stiffness dynamics," *Biological Cybernetics,* vol. 80, no. 5, pp. 327-337, May 1999.

[14] D. W. Franklin, G. Liaw, T. E. Milner, R. Osu, E. Burdet, and M. Kawato, "Endpoint stiffness of the arm is directionally tuned to instability in the environment," *J Neurosci,* vol. 27, no. 29, pp. 7705-16, Jul 18 2007.

[15] M. A. Krutky, R. D. Trumbower, and E. J. Perreault, "Influence of environmental stability on the regulation of end-point impedance during the maintenance of arm posture," *Journal of Neurophysiology,* vol. 109, no. 4, pp. 1045-1054, Feb 2013.

[16] E. Burdet, R. Osu, D. W. Franklin, T. E. Milner, and M. Kawato, "The central nervous system stabilizes unstable dynamics by learning optimal impedance," *Nature,* vol. 414, no. 6862, pp. 446-9, Nov 22 2001.

[17] E. J. Perreault, R. F. Kirsch, and P. E. Crago, "Effects of voluntary force generation on the elastic components of endpoint stiffness," *Exp Brain Res,* vol. 141, no. 3, pp. 312-23, Dec 2001.

[18] H. Hanzlick, H. Murphy, and H. Lee, "Stability of the Human Ankle in Relation to Environmental Mechanics," in *In Proc. IEEE International Conference on Robotics and Automation (ICRA 2017)*, Singapore, 2017.

[19] A. Goswami, B. Thuilot, and B. Espiau, "Compas-like biped robot Part I: Stability and bifurcation of passive gaits," *INRIA,* vol. 2996, 1996.

[20] H. Hanzlick and L. Hyunglae, "Gender difference of ankle stability in the sagittal and frontal planes," *Conf Proc IEEE Eng Med Biol Soc,* vol. 2017, pp. 1621-1624, Jul 2017.

[21] H. Lee and N. Hogan, "Essential considerations for design and control of human-interactive robots," in *In Proc. 2016 IEEE International Conference on Robotics and Automation (ICRA 2016)*, Stockholm, 2016, pp. 3069-3074.

[22] R. E. Kearney and I. W. Hunter, "System-Identification of Human Joint Dynamics," *Critical Reviews in Biomedical Engineering,* vol. 18, no. 1, pp. 55-87, 1990.

[23] H. Lee, H. I. Krebs, and N. Hogan, "Multivariable Dynamic Ankle Mechanical Impedance with Active Muscles," *IEEE Transactions on Neural Systems and Rehabilitation Engineering,* vol. 22, no. 5, pp. 971-981, Sep 2014.

[24] H. Lee and E. J. Perreault, "Stabilizing stretch reflexes are modulated independently from the rapid release of perturbation-triggered motor plans," *Sci Rep,* vol. 9, no. 1, p. 13926, Sep 26 2019.

[25] J. Arnold, H. Hanzlick, and H. Lee, "Variable Damping Control of the Robotic Ankle Joint to Improve Trade-off between Performance and Stability," in *IEEE International Conference on Robotics and Automation (ICRA)*, Montreal, Canada, 2019, pp. 1699-1704.

[26] T. Bitz, F. Zahedi, and H. Lee, "Variable Damping Control of a Robotic Arm to Improve Trade-off between Agility and Stability and Reduce User Effort," in *IEEE International Conference on Robotics and Automation (ICRA)*, France, 2020.